Direct multi-channel optical spectrum analysis of radio-wave signals using collinear wave heterodyning in the single acousto-optical cell

To cite this article: Alexandre S Shcherbakov *et al* 2010 *J. Opt.* **12** 045203

View the article online for updates and enhancements.

IOP ebooks™

Bringing you innovative digital publishing with leading voices to create your essential collection of books in STEM research.

Start exploring the collection - download the first chapter of every title for free.

Direct multi-channel optical spectrum analysis of radio-wave signals using collinear wave heterodyning in the single acousto-optical cell

Alexandre S Shcherbakov[1], **D Sanchez Lucero**[1],
A Luna Castellanos[1] **and Olga I Belokurova**[2]

[1] National Institute for Astrophysics, Optics, and Electronics (INAOE), A.P. 51 y 216,
Puebla 72000, Mexico
[2] St Petersburg State Polytechnic University, Polytechnicheskaya Street 29,
Saint Petersburg 195251, Russian Federation

E-mail: alex@inaoep.mx, danielslfce@yahoo.com.mx, aluna@inaoep.mx and
obelokurova@mail.ru

Abstract
An attempt is made to improve the accuracy of a multi-channel parallel acousto-optical
spectrum analysis through involving an additional nonlinear conversion into data processing.
For this purpose we investigate the potential of exploiting a co-directional collinear wave
heterodyning within an analysis of ultra-high-frequency radio-wave signals. The wave
heterodyning under the proposal is performed via mixing the longitudinal elastic waves of finite
amplitudes. It leads to a two-cascade processing in the single-crystalline cell and makes it
possible to improve the relative frequency resolution of the acousto-optical spectrum analysis
by an order of magnitude at the same frequency range. Both the theoretical findings and the
corresponding estimations were used in proof-of-principle experiments directed at creating a
new type of acousto-optical cell. The general concept of the proposed method and the basic
conclusions are confirmed by experiments with the developed acousto-optic cell made of a lead
molybdate crystal.

Keywords: acousto-optical spectrum analysis, frequency resolution, collinear wave
heterodyning

1. Introduction

A significant part of recent progress in optical data processing
is related to exploiting various nonlinear phenomena including,
for instance, soliton propagation, parametric processes,
etc [1, 2]. An opportunity for implementing a two-cascade
processing for binary encoded digital data based on three-
wave interactions between coherent waves of different natures
(optical and non-optical) has recently been considered [3].
In line with this, we now study potential possibilities related
to using a collinear wave mixing in the specific case of a
medium without any group-velocity dispersion while with
strongly dispersive losses. Our approach allows us to realize

effective wave heterodyning, when the beneficial data in the
signal becomes converted from a relatively high-frequency
carrier wave to a difference-frequency wave. The accuracy
of spectral as well as frequency measurements is physically
determined by the uncertainty in the energy or momentum
inherent in a photon localized in the interaction area [4]. Due
to a rather strong dispersion of losses, the heterodyning leads
to increasing the characteristic length and time of propagation
(they are both associated with a clear optical aperture) for the
converted signal in that medium and to improving significantly
the accuracy of signal processing. In this context, we present
our results in the real-time optical analysis of frequency
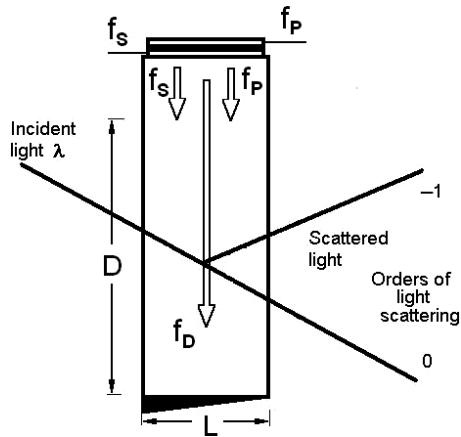spectra, belonging to analog ultra-high-frequency radio-wave

Figure 1. Schematic arrangement of the interacting beams in a two-cascade cell.

signals, with considerably improved frequency resolution. These results are based on a two-cascade processing, i.e. on exploiting a pair of different wave processes one after the other sequentially in the single-crystalline cell. This cell includes two resonant piezoelectric transducers, converting the input electronic signals into gigahertz-frequency elastic waves, with the corresponding electronic ports on its upper facet, clear optical aperture D and an effective acoustic absorber on its bottom facet, see figure 1.

The first wave process represents mixing the longitudinal elastic waves of finite amplitudes in a compactly localized upper domain of a cell where the relatively powerful pump of the frequency f_P interacts with the relatively weaker signal elastic wave of the frequency f_S. During just this nonlinear process a collinear wave heterodyning takes place providing the appearance of an elastic wave of the difference frequency f_D, which is able to propagate along a large-aperture cell due to weaker manifestation of strongly dispersive losses at lower frequencies. The second wave process is the subsequent Bragg light scattering by the difference-frequency elastic wave in a possible linear regime, i.e. in the regime of a given acoustic field for the incident light beam. This process occurs within a clear aperture D illuminated by a wide incident optical beam of wavelength λ and is able to realize optical spectrum analysis by itself. When, for example, the signal wave is rather intricate in behavior and consists of various frequencies, each individual spectral component from the difference-frequency elastic wave plays the role of a partial thick dynamic diffractive grating for the incident light beam. The length L of the acousto-optical interaction has to provide performing the Bragg regime of light scattering.

In frames of the studies carried out, the technique of substantial approximations has been used to develop a theoretical description, which governs the difference-frequency elastic wave and adapts the corresponding expressions related to the light scattering. These findings make it possible first to estimate potential efficiencies for both the above-mentioned wave processes in optically transparent medium with square-law nonlinearity and dispersive acoustic losses. Then, analyzing the frequency properties and physical limitations gives us an

opportunity to formulate requirements for performance data of the acousto-optical cell as well as for acceptable values of the operating frequencies. After that, the progressed theory is used in our experimental studies aimed at improving the accuracy of a multi-channel parallel optical data processing by an order of magnitude. In so doing, the acousto-optical spectrum analysis of a gigahertz-frequency-range radio-wave signals with essentially improved frequency resolution is realized and investigated. During our proof-of-principle experiments a new type of acousto-optical cell made of a rather effective lead molybdate single crystal was exploited. These preliminary experimental data show that the elaborated approach, based algorithmically on a two-cascade processing, allows us a direct multi-channel parallel optical analysis of spectra inherent in ultra-high-frequency radio-wave signals at a relative accuracy of about 10^{-4}.

2. Potential efficiency of the processing

It is well known that co-directional collinear propagation of the longitudinal acoustic waves of finite amplitudes along the acoustic axes in crystals, which do not have the group-velocity dispersion but exhibit a square-law dispersive linear dissipation, is governed by the Burgers equation for the normalized elastic distortion $\xi = D_1/D_0$ [5]:

$$\frac{\partial \xi}{\partial y} = B\xi \frac{\partial \xi}{\partial \theta} + \frac{\partial^2 \xi}{\partial \theta^2}. \tag{1}$$

Here, D_1 and D_0 are the current and maximal amplitudes of elastic distortion, $\theta = 2\pi f_P(t - x/V)$, x and t are the laboratory coordinates; $y = \alpha_P x$, $f_P V$ and α_P are the frequency, velocity and logarithmic attenuation of the initially pumping acoustic wave. The dimensionless parameter $B = -\pi f_P \Gamma D_0/(\alpha_P V)$ describes a ratio of the nonlinearity to the dissipation; Γ is the acoustic nonlinearity constant. Generally, equation (1) can be solved analytically with arbitrary boundary conditions due to Hopf–Cole transformation converting equation (1) into the heat conduction equation [5]. However, the very cumbersome form of such a solution does not allow the subsequent harmonic analysis. That is why finding an approximate solution by the method of successive approximations is the most worthwhile when the parameter B is not too large. In so doing, let us take the boundary condition to equation (1) in the form of a superposition of two waves $\xi(y = 0, \theta) = \sin(\theta + \psi) + \delta \sin(\gamma \theta)$. The first term with the unit amplitude and the frequency f_P is the pump, while the other one represents a signal with amplitude δ and frequency f_S. Here $\gamma = f_S/f_P$, ψ is the initial phase shift between the signal and pump waves, $\delta = \sqrt{P_S/P_P}$, P_P and P_S are the acoustic power densities for a pump and signal, respectively. Thus, the maximal amplitude of pump distortion in a medium, whose material density is ρ, can be expressed as $D_0 = \sqrt{2P_P/(\rho V^3)}$. Substituting $\xi(y = 0, \theta)$ into equation (1), one can find the zero approximation describing the propagation of two attenuating and non-interacting waves $\xi^{(0)} = \exp(-y)\sin(\theta + \psi) + \delta \exp(-\gamma^2 y)\sin(\gamma \theta)$. Now,
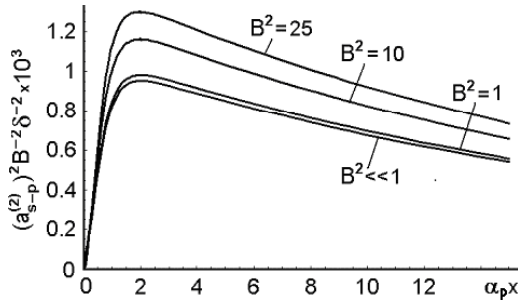
Figure 2. The spatial normalized plots for the difference-frequency acoustic wave power in the second approximation for various values of the parameter B with $\gamma = 1.15$ and $\delta^3 \ll 1$.

using $\xi^{(0)}$ only in the nonlinear term of equation (1), one can get the first approximation solution to equation (1) as

$$\xi^{(1)} = \xi^{(0)} + a_{P+P}^{(1)} \sin[2(\theta + \psi)] + a_{S+S}^{(1)} \sin(2\gamma\theta)$$
$$+ a_{S+P}^{(1)} \sin[(\gamma + 1)\theta + \psi] + a_{S-P}^{(1)} \sin[(\gamma - 1)\theta + \psi]. \quad (2)$$

Here, $a_{P+P}^{(1)}$ and $a_{S+S}^{(1)}$ are the amplitudes for the second harmonics of pump and signal waves, $a_{S+P}^{(1)}$ and $a_{S-P}^{(1)}$ give the amplitudes of acoustic waves with the combined and difference frequencies. Within our further considerations, only the difference-frequency acoustic wave will be used. When the nonlinearity does not exceed the dissipation in a system, i.e. $B^2 \leqslant 1$, and together with this when $\delta^3 \ll 1$, the difference-frequency wave amplitude is given by

$$a_{S-P}^{(1)}(x) = B\delta \left(\frac{\gamma - 1}{4\gamma} \right) [1 - \exp(-2\gamma\alpha_P x)]$$
$$\times \exp[-\alpha_P x (1 - \gamma)^2]. \quad (3)$$

The performed analysis has shown that possible corrections to the first-order solution $a_{S-P}^{(1)}$ increase the difference-frequency acoustic wave amplitude. By this is meant that, when $B^2 \sim P_P$ grows, for instance, by ten times, the resulting power at the difference frequency shows an increase by more then ten times, see figure 2. Nevertheless, including the obtained correction of second order in the solution of the first-order approximation changes nothing in the character of these dependences and leads to only slight numerical additions with $B^2 \leqslant 1$.

The power density P_D of the difference-frequency wave can be explained from equation (3) as

$$P_D(\gamma, \alpha_P x) = P_P P_S \left(\frac{f_D}{f_P f_S} \right)^2 m[1 - \exp(-2\gamma\alpha_P x)]^2$$
$$\times \exp[-2\alpha_P x (1 - \gamma)^2], \quad (4)$$

where $f_D = |f_P - f_S|$. Then, the factor $m = \pi^2 \Gamma^2 / (8\rho V^5 \tilde{\Gamma}_0^2)$ includes only a set of parameters inherent in the chosen medium and determines the efficiency of producing the difference-frequency acoustic wave in this medium. Usually, the attenuation factor Γ_0 is mentioned in the bibliography (see [6, 7]) in units of dB cm^{-1} GHz^{-2}, but here one needs it in the form of $\tilde{\Gamma}_0$ (s^2 cm^{-1}) $= [(\ln 10)/10] \times 10^{-18} \times \Gamma_0$ (dB cm^{-1} GHz^{-2}) within estimating the power density.

Now, let us discuss the efficiency I of Bragg light scattering by the difference-frequency acoustic wave. In the

case of weak acoustic signals, when nonlinearity inherent in acousto-optical interaction can be omitted [8], one can use the following expansion:

$$I = \sin^2(qL) \approx q^2 L^2 - \tfrac{1}{3} q^4 L^4 + \cdots, \quad (5a)$$

$$q \approx \pi\lambda^{-1}\sqrt{M_2 P_D/2}. \quad (5b)$$

Here, λ is the light wavelength in the air. The figure $M_2 = n^6 p_{\text{eff}}^2 / (\rho V^3)$ of acousto-optical merit for the chosen crystal includes the refractive index n and the effective photo-elastic constant p_{eff}, which both depend on the crystal cut. Under the condition $q^2 L^2 \ll 3$, i.e. within

$$P_D \ll 6\lambda^2 / (\pi^2 M_2 L^2), \quad (6)$$

one may take only the first term in equation (5a). Exploiting equation (4), one can rewrite equation (5a) as

$$I = \frac{\pi^2 M_2 L^2}{2\lambda^2} P_P P_S \left(\frac{f_D}{f_P f_S} \right)^2 m[1 - \exp(-2\gamma\alpha_P x)]^2$$
$$\times \exp[-2\alpha_P x (1 - \gamma)^2], \quad (7)$$

which determines the combined efficiency of the acousto-optical cell under consideration in terms of light scattering. Now, the potential efficiency I of Bragg light scattering by the difference-frequency acoustic wave has to be estimated in a lead molybdate (PbMoO$_4$) single crystal; symmetry (4/m). The crystal allows the existing pure longitudinal elastic mode with velocity $V = 3.62 \times 10^5$ cm s^{-1} when this elastic wave is passing along the [001] axis. Such an orientation has its original motivation in preliminary data related to linear and nonlinear manifestations of optical and acoustical properties inherent in this crystal. In particular, it exhibits rather high efficiency of collinear interaction for the longitudinal acoustic waves in the [001] direction described by $|\Gamma| = 17.5$ [6, 7]. Then, a maximal figure of acousto-optical merit $M_2 = 40.4 \times 10^{-18}$ s^3 g^{-1} is inherent in just normal light diffraction in the (110) plane.

Now, the contribution of an acousto-optical interaction should be estimated. The Bragg regime of light diffraction occurs when the angle of light incidence on the acoustic grating meets the corresponding Bragg condition and the inequality $Q = 2\pi\lambda L f_D^2 / (nV^2) \gg 1$ for the Klein–Cook parameter Q [9] is satisfied. Taking $\lambda = 532$ nm, $n \approx 2.26$ (in PbMoO$_4$), $L = 1.0$ cm and $f_D = 60$ MHz, one can estimate $Q \approx 4.04$. Hence, the regime of light scattering, which is rather close to the Bragg regime at least in a small-signal linear region, could be expected for the acoustic different frequencies of about 60 MHz. Using equation (6), the contribution of the acousto-optical interaction can be sufficiently accurate estimated from the first term of equation (5a):

$$I_{\max} = \pi^2 M_2 L^2 P_{D\max} / (2\lambda^2). \quad (8)$$

With the maximally allowed level $P_{D\max} \approx 4.5 \times 10^6$ g s^{-3} = 0.45 W cm^{-2} obtained from equation (6), one can find $I_{\max} \approx 0.3$. This estimation makes it possible to consider the level of P_D chosen above as more or less tolerable for an upper limit in lead molybdate under the aforementioned
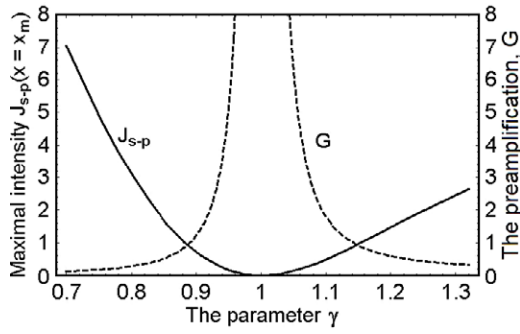
Figure 3. Plots of the maximal intensity $J_{S-P}(x = x_m)$ and the preamplification $G(\gamma; \gamma_0 = 1.17)$ versus the parameter γ for the magnitudes of γ practically usable within the wave heterodyning.

condition given by equation (6). An undoubted merit of this characterization consists in practically convenient direct proportionality between the efficiency I and the power density P_D. At the second step, the contribution of acoustic wave mixing should be briefly analyzed. With this object in view, one can use equation (4) for estimating the acoustic pump power density P_{P0} needed to reaching a pre-assigned peak level of the difference-frequency power density $P_{D\,max}$ within $\delta^3 \ll 1$ at a given ratio $\alpha = P_S/P_{P0}$. From the start, it can be easily shown that a peak magnitude peculiar to the coordinate dependence in equation (4) is close to unity, i.e. $\text{Max}\{[1 - \exp(-2\gamma\alpha_P x)]^2 \exp[-2\alpha_P x(1 - \gamma)^2]\} \cong 1$. Consequently, one can find

$$P_{P0} = \frac{f_S}{|1 - \gamma|}\sqrt{\frac{P_{D\,max}}{\alpha m}}. \qquad (9)$$

Let us consider an illustrative example for PbMoO$_4$ when $I_{max} = 3\%$ (which is quite natural for the spectrum analysis in a small-signal linear regime), so that equation (6) gives $P_{D\,max} \approx 4 \times 10^5 \text{ g s}^{-3} = 40 \text{ mW cm}^{-2}$. Taking $m = 7.25 \times 10^8 \text{ s g}^{-1}$, $\alpha = 0.1$, $\gamma = 1.15$ and $f_S = 1.0$ GHz, one can find $P_{P0} \approx 50 \times 10^7 \text{ g s}^{-3} = 50 \text{ W cm}^{-2}$ and $P_S \approx 5.0 \text{ W cm}^{-2}$. These estimations do not look unacceptable practically and can be improved with using more effective materials.

3. Estimating the frequency potentials peculiar to a novel acousto-optical cell

The normalized intensity $J_{S-P}(x) = [a_{S-P}^{(1)}(x)]^2 B^{-2} \delta^{-2}$ of the difference-frequency acoustic wave passing along the cell's optical aperture can be found from equation (3) in the form

$$J_{S-P}(x) = \left(\frac{\gamma - 1}{4\gamma}\right)^2 [1 - \exp(-2\gamma\alpha_P x)]^2$$
$$\times \exp[-2\alpha_P x(1 - \gamma)^2]. \qquad (10)$$

From equation (10), one can find the point x_m associated with the absolute maximum of the normalized intensity distribution inherent in the acoustic wave along the total cell's optical aperture as

$$x_m = \left(\frac{-1}{2\alpha_P\gamma}\right) \ln\left[\frac{(1 - \gamma)^2}{1 + \gamma^2}\right]. \qquad (11)$$

The magnitude of this maximum can be estimated at the point x_m as

$$J_{S-P}(x = x_m) = \frac{(\gamma - 1)^2}{4(1 + \gamma^2)^2} \exp\left\{\frac{(1 - \gamma)^2}{\gamma} \ln\left[\frac{(1 - \gamma)^2}{1 + \gamma^2}\right]\right\}. \qquad (12)$$

It is seen from equation (12) and figure 2 that the normalized intensity $J_{S-P}(x = x_m)$ is a function of γ, see the solid line in figure 3. However, such a dependence on γ leads to a non-uniformity of distributing signals associated with various difference-frequency components inside the cell. To compensate this non-uniformity one can suggest exploiting the additionally needed preamplification $G(\gamma; \gamma_0)$, which can be calculated as

$$G(\gamma; \gamma_0) = \frac{3J_{S-P}(x = x_m, \gamma = \gamma_0)}{4J_{S-P}(x = x_m, \gamma)}, \qquad (13)$$

where γ_0 is initially selected and the fixed value of the ratio γ. This fixed γ_0 can be minimal or maximal, depending on the case $\gamma < 1$ or $\gamma > 1$ is chosen. An example of the needed preamplification $G(\gamma; \gamma_0)$ with $\gamma_0 = 1.17$ is shown by the dashed line in figure 3. Decreasing the normalized intensity $J_{S-P}(x = x_m)$ down to a level of -3 dB along the optical aperture at a point x_D gives the equality $J_{S-P}(x = x_D) = (1/2)J_{S-P}(x = x_m)$, so that one can find

$$x_D = \frac{-1}{2\alpha_P(1 - \gamma)^2}\left(\ln\left(\frac{\gamma\sqrt{2}}{1 + \gamma^2}\right) + \left\{\frac{(1 - \gamma)^2}{2\gamma} \ln\left[\frac{(1 - \gamma)^2}{1 + \gamma^2}\right]\right\}\right). \qquad (14)$$

In fact, the magnitude of x_D determines the total length of the acousto-optical cell with the collinear wave heterodyning. Now, the really operating part D of the cell's optical aperture available for optical processing can be found as

$$D = x_D - x_m = \frac{F(\gamma)}{\alpha_P}, \qquad (15a)$$

$$F(\gamma) = \frac{1}{(1 - \gamma)^2} \ln\left(\frac{1 + \gamma^2}{\gamma\sqrt{2}}\right), \qquad (15b)$$

where the amplitude decrement is given by α_P (cm^{-1}) $= 0.115 \times \Gamma_0[f_P$ (GHz)$]^2$. Consequently, the following expressions for the pump frequency f_P and for the difference frequency f_D (where $f_D = f_P - f_S = f_P(1 - \gamma)$ if $\gamma < 1$ or $f_D = f_S - f_P = f_P(\gamma - 1)$ if $\gamma > 1$) appear:

$$f_P = \sqrt{\frac{F(\gamma)}{0.115\Gamma_0 D}}, \qquad (16a)$$

$$f_D = |1 - \gamma|\sqrt{\frac{F(\gamma)}{0.115\Gamma_0 D}}. \qquad (16b)$$

Now, let us direct our attention to the particular case of a lead molybdate crystalline cell ($\Gamma_0 = 15$ dB cm^{-1} GHz^{-2}) with a practically available optical aperture $D = 3.7$ cm and make a few estimations. At first, to provide higher operating frequencies together with the simplicity of realizing a low-frequency pump one can take an area of $\gamma > 1$ with $f_D = $
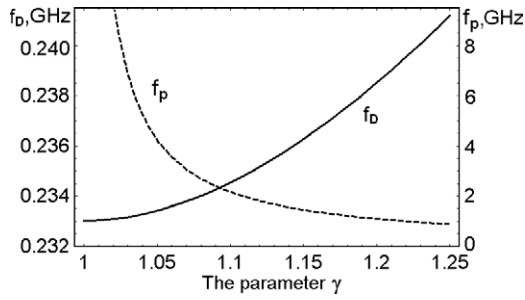
Figure 4. Plots for the pump frequency f_P (dashed line) and the difference frequency f_D (solid line) related to equations (16) versus γ for magnitudes of γ practically usable in the wave heterodyning.

Figure 5. Non-uniformities in the distributions of signals associated with various difference-frequency acoustic wave components in the lead molybdate cell.

$f_S - f_P = f_P(\gamma - 1)$. It could be chosen in spite of the facts that the efficiency of frequency conversion in an area of $\gamma \in [0.70, 0.95]$ exceeds by a little bit the efficiency for $\gamma \in [1.05, 1.30]$ and one will be in need of slightly higher preamplification with $\gamma > 1$. Applying equations (16) to a lead molybdate cell with $D = 3.7$ cm and $\gamma > 1$, one can obtain the diagram shown in figure 4.

These dependences allow the following estimations for practical realization. Let us take the upper difference frequency as $f_{UD} = 236$ MHz and the upper magnitude of γ as $\gamma_U = 1.17$, so that from equation (16a) the pump frequency will be $f_P = 1388$ MHz and the upper signal frequency will be $f_{US} = 1624$ MHz. Then, one can choose the bandwidth Δf of analysis, for example, in the range of 180 MHz, which leads to the lower difference frequency $f_{LD} = 56$ MHz restricted by the Bragg regime condition, see section 2. Consequently, the lower signal frequency is $f_{LS} = 1444$ MHz and the lower magnitude of γ is $\gamma_L = 1.04$. These estimations are conditioned by the following relations:

$$f_{UD} = f_{US} - f_P = f_P(\gamma_U - 1), \qquad (17a)$$

$$f_{LD} = f_{LS} - f_P = f_P(\gamma_L - 1). \qquad (17b)$$

It should be noted that direct exploitation of a similar lead molybdate cell with the active optical aperture $D = 3.7$ cm at the signal frequencies of about 1000 MHz is definitely impossible, because the acoustic attenuation exceeds 55 dB along this aperture. Nevertheless, applying the collinear acoustic wave heterodyning allows us to operate on these gigahertz-range carrier frequencies. Non-uniformities in the distributions of signals are illustrated in figure 5, where $G = 1$ for $\gamma_U = 1.17$ and $G = 6$, as it follows from equations (16) and figure 3 for $\gamma_L = 1.04$. Using equation (11), one can estimate that $x_m = 0.58$ cm for $\gamma_U = 1.17$ and $x_m = 0.94$ cm for $\gamma_U = 1.04$ with $\alpha_P = 3.32$ cm^{-1}. Figure 6 shows that the real operating optical aperture D lies between $x = 0.4$ and 4.2 cm for $\gamma_U = 1.17$, resulting in at least $D \approx 3.8$ cm. The physical limit for potential frequency resolution of a cell is given by the value $\delta f \approx V/D$.

4. Characterizing the optical part of experimental set-up and some practical estimations

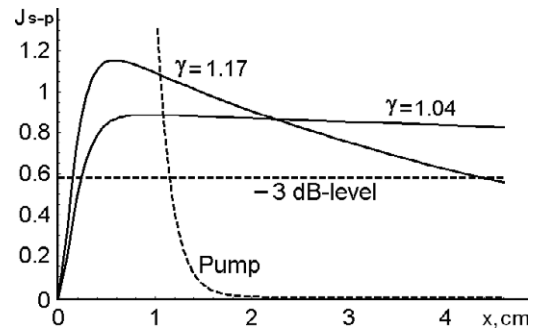Exploiting the above-listed estimations, a novel acousto-optical cell had been designed and used in an almost standard optical scheme for acousto-optical spectrum analysis of gigahertz-frequency range radio signals, see figure 6. This scheme includes a green-light laser ($\lambda = 532$ nm, the output optical power exceeds 100 mW), a four-prism beam expander (only two of them are shown), a rectangular selecting optical diaphragm, a single-crystal acousto-optical cell with acoustic absorber and two ultra-high-frequency electronic ports for the input signal and pump, a large-aperture achromatic doublet lens and a 3000-pixel CCD linear array camera. A lead molybdate single crystal of 42 mm in total length, oriented as has been described above, was used in that cell. The incident light was linearly polarized along the [0, 0, 1] axis of the cell's crystal. It provided, on the one hand, the maximal transmission of the prism beam expander due to coincidence of the plane of expanding laser beam with the corresponding vector of light polarization and, on the other hand, the maximal efficiency of the acousto-optical interaction in a lead molybdate single crystal (see section 2).

The size of an individual resolvable spot can be remarkably affected by a non-uniformity of the light stream leaving the acousto-optical cell output facet. This non-uniformity was governed by a combined distribution of the incident light field profile and the declining distribution of the difference-frequency acoustic wave along the cell's optical aperture. Usually, the profile of the incident light field is close to a Gaussian shape, because it is conditioned, first of all, by the initial profile of the laser beam. Together with this, just a Gaussian profile is commonly used within possible apodization of the incident beam profile. In addition, the apodization is originally directed at suppressing the side lobes, which are peculiar to the light distribution of each individual resolvable spot in a Fourier transform plane of the integrating lens. In so doing, the apodization is capable of increasing the potential dynamic range of spectrum analysis. Reasoning from the assumption that the electric field profile E_{in} reaching the cell's optical aperture has a Gaussian shape, one can write (in both physical and dimensionless variables) that

$$E_{in} = E_0 \exp[-\sigma(x_1 - x_0)^2] = E_0 \exp[-\beta(y - y_0)^2],$$

$$I_{in} = E_{in}^2, \qquad (18)$$

where x_1 and D are the physical coordinates across a beam and the physical cell's optical aperture measured in centimeters,
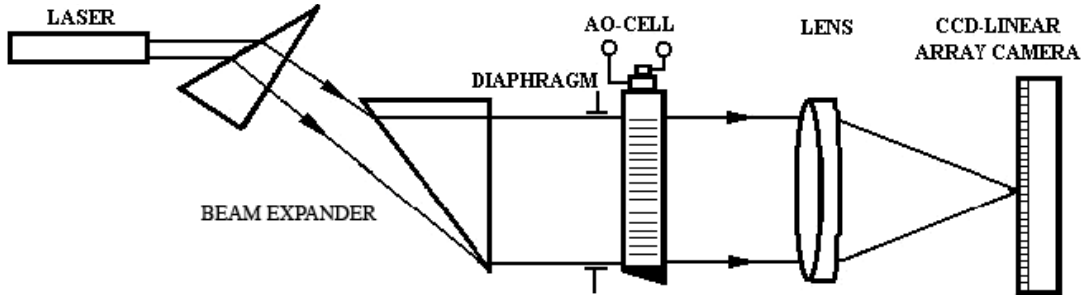
Figure 6. Scheme of the acousto-optical spectrum analyzer with collinear wave heterodyning.
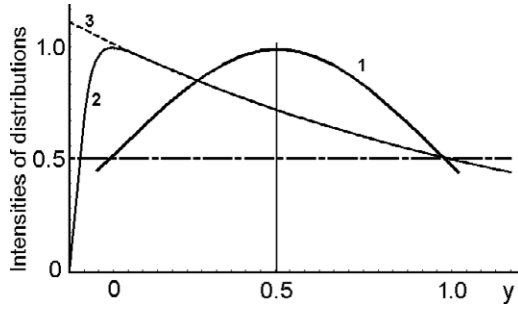

Figure 7. Intensity distributions for Gaussian profile of the incident light with $\beta = 1.382$ (bold line 1) as well as for the difference-frequency acoustic wave with $\alpha_D \approx 0.345$, $\gamma_U = 1.17$ (solid line 2) along optical cell's aperture. For the comparison, the dependence reflecting equations (19) is shown (dashed line 3).

$y = x_1/D$ is the normalized dimensionless coordinate, so that the coordinates x_0 and y_0 correspond to the center of the distribution, σ and $\beta = \sigma D^2$ are physical and dimensionless parameters of the Gaussian shape function.

Generally, the declining intensity distribution of the difference-frequency acoustic wave along the cell's optical aperture is characterized by equation (4) and it has to be taken into account in the framework of our analysis. However in an area of the clear optical aperture $D = x_D - x_m$, one can take only the reduced expression $a_{S-P}^{(1)}(x) \propto \exp[-\alpha_P x(1 - \gamma)^2]$ with $x \in [x_m, x_D]$. To have a chance of joining this formula with equations (18) one has to determine $x_1 = x - x_m$ and to normalize $a_{S-P}^{(1)}(x)$ by its magnitude just at the point x_m. As a result, one can write

$$a_{S-P}^{(N)} = \exp[-\alpha_P x_1(1 - \gamma)^2] = \exp[-\alpha_D y],$$
$$J_{S-P}^{(N)} = [a_{S-P}^{(N)}]^2, \tag{19}$$

where the amplitude decrement $\alpha_D = \alpha_P D(1 - \gamma)^2$ describes a total value of losses over all of the cell's optical aperture D for the difference-frequency acoustic wave; it can be expressed in decibels or in a dimensionless form, because α_P (cm^{-1}) $= 0.115 \times \alpha_P$ (dB cm^{-1}). To illustrate a sense of this reasoning let us consider the following example. Taking $y_0 = 0.5$ and formulating the condition $I_{in}(y = 0) = I_{in}(y = 1) = 0.5 \times I_{in}(y = 0.5)$, one can find that the needed dimensionless parameter of the Gaussian-shape function is $\beta = 1.382$. Then, assuming that $J_{S-P}^{(N)}(y = 1) = 0.5 \times J_{S-P}^{(N)}(y = 0)$, one can estimate $\alpha_D \approx 0.345$ in the worst case of $\gamma_U = 1.17$. The

plots corresponding to this example are presented in figure 7. The total intensity of the light field passing through the cell's aperture can be estimated by the value

$$I_A = \left[\int_0^1 \exp[-\beta(y - 0.5)^2] \exp(-\alpha_D y) \, dy \right]^2$$
$$= \frac{\pi}{4\beta} \exp\left[\frac{\alpha_D}{2\beta}(\alpha_D - 2\beta) \right]$$
$$\times \left[\text{Erf}\left(\frac{\alpha_D + \beta}{2\sqrt{\beta}} \right) - \text{Erf}\left(\frac{\alpha_D - \beta}{2\sqrt{\beta}} \right) \right].$$

The shape of the light field distribution $E(u)$ (the dimensionless coordinate u is centered on a maximum of this distribution) peculiar to an individual resolvable spot in a Fourier transform plane of the integrating lens can be estimated analytically as

$$E(u) = \int_0^1 \exp[-\beta(y - 0.5)^2] \exp(-\alpha_D y) \exp(-2i\pi u y) \, dy$$
$$= \frac{1}{2} \sqrt{\frac{\pi}{\beta}} \exp\left[-\beta\left(\frac{1}{4} - \nu^2 \right) \right]$$
$$\times \{ \text{Erf}[\sqrt{\beta}(1 + \nu)] - \text{Erf}[\sqrt{\beta}\nu] \}, \tag{20}$$

where the notation $\nu = (\alpha_D/2\beta - 1/2) + i\frac{\pi u}{\beta}$ is used. Let us introduce $\nu(u = 0) = \nu_0 = (\alpha_D/2\beta - 1/2)$ and obtain

$$E(u = 0) = \frac{1}{2} \sqrt{\frac{\pi}{\beta}} \exp\left[-\beta\left(\frac{1}{4} - \nu_0^2 \right) \right]$$
$$\times \{ \text{Erf}[\sqrt{\beta}(1 + \nu_0)] - \text{Erf}[\sqrt{\beta}\nu_0] \}, \tag{21}$$

which is real-valued in behavior. Using equations (20) and (21), the normalized distribution $I(u)$ of light intensity peculiar to an individual resolvable spot in a Fourier transform plane of the integrating lens can be written as $I(u, \beta, \alpha_D) = E(u)E^*(u)E^{-2}(u = 0)$. Generally, $u = wD/\lambda F_L$, where w is the physical spatial coordinate in the focal plane and F_L is the focal distance of the integrating lens. In the particular case of $\beta \equiv 0$, one can find

$$I(u, \beta = 0, \alpha_D) = \frac{\sin^2(\pi u) + \sinh^2(\alpha_D/2)}{[1 + (2\pi u/\alpha_D)^2]\sinh^2(\alpha_D/2)}. \tag{22}$$

Results of numerical simulations for $I(u, \beta, \alpha_D)$, based on equations (20)–(22), with practically useful values of β and α_D are shown in figure 8. It is seen from figure 8 that increasing the amplitude decrement α_D leads to growing of the side lobes and minima of the normalized light intensity distribution inherent in each individual resolvable spot in the focal plane of the integrating lens. Moreover, the spatial width of the main lobe
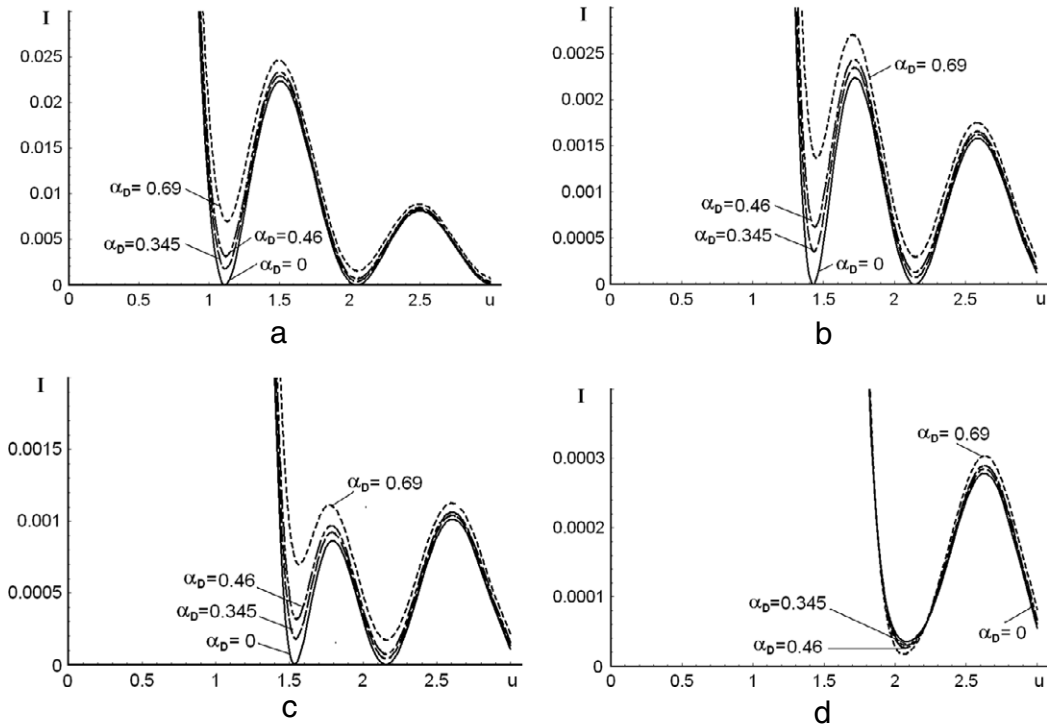
Figure 8. The combined effect of both the incident light apodization and the acoustic beam attenuation on the normalized light intensity in the focal plane of the integrating lens: (a) is for $\beta = 2$, (b) is $\beta = 6$, (c) is for $\beta = 7$ and (d) is for $\beta = 10$; here, various vertical scales are taken for each magnitude of β.

peculiar to each individual resolvable spot shows an increase due to the presence of losses, so that the real magnitude of the frequency resolution δf is moving away from the limit V/D. Together with this, increasing the parameter β provides suppressing side lobes and minima of light distributions, so that as usual the dynamic range could be increased. Then, one can see from figures 8(b) and (c) that, for magnitudes of β exceeding some value, which has been estimated by about 6.7, the second side lobe dominates over the first one. This fact and a tendency to broadening the main lobe due to losses are illustrated in figure 9 in the particular case of $\alpha_D = 0.345$.

Now, let us estimate potential possibilities related to both the dynamic range and the width of an individual resolvable spot in a scheme of an acousto-optical spectrometer with a co-directional collinear wave heterodyning. The most critical limitation for the dynamic range is related to the maximal level of side lobes. Figure 10 illustrates affecting the dynamic range by a maximal side lobe, so that one can clearly see that acoustic attenuation decreases the potential dynamic range, which grows by itself on increasing the parameter β. Broadening the main lobe of an individual resolvable spot is characterized by the third curve in figure 10, which reflects increasing its width at a level of 0.405 corresponding to the Rayleigh resolution criterion [10].

5. Proof-of-principle experimental studies of optical spectrum analysis with a novel lead molybdate crystalline acousto-optical cell

As has been mentioned above, a novel acousto-optic cell was made of a lead molybdate single crystal and completed
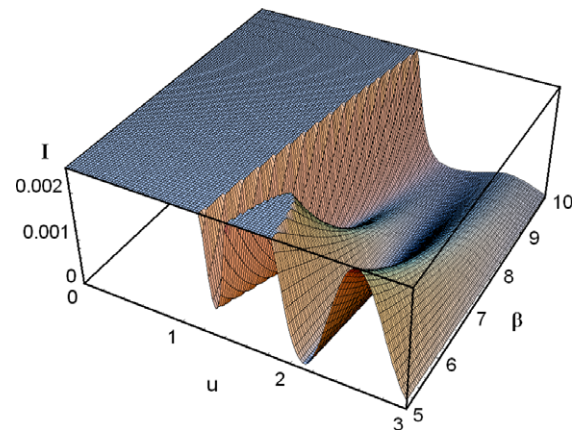

Figure 9. The general plot of the light intensity distribution inherent in an individual resolvable spot in a Fourier plane with $\alpha_D = 0.345$ and $\beta \in [5, 10]$.

(This figure is in colour only in the electronic version)

with a pair of electronic input ports for the pump and signal on one of its facets as well as with an acoustic absorber on the opposite facet. The piezoelectric transducer with an interaction length of 1.0 cm, generating a signal wave with a power density of about 100 mW mm^{-2}, was made of a thin $(Y + 36°)$-cut lithium niobate crystal, so that it excited a purely longitudinal acoustic wave, with conversion losses of about 2 dB at its resonant frequency close to 1530 MHz. The single-frequency pumping longitudinal acoustic wave with a power density of up to 600 mW mm^{-2} was generated at a carrier frequency of approximately 1390 MHz, so that the case of
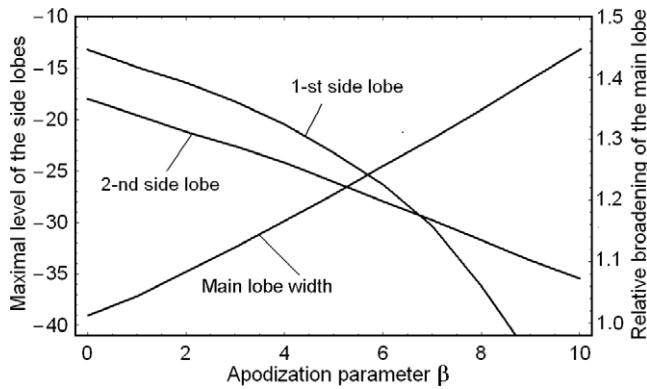
Figure 10. Width of the main lobe at a level of 0.405 and maximal levels of the side lobes, the first or second ones, versus the apodization parameter β with $\alpha_D = 0.345$.

Figure 12. The digitized profile of an individual resolvable spot inherent in a PbMoO$_4$ cell with the most non-uniform ($\gamma_U = 1.17$) distribution of the difference-frequency wave along a 3.7 cm aperture; horizontal lines are spaced by 2.5 dB.
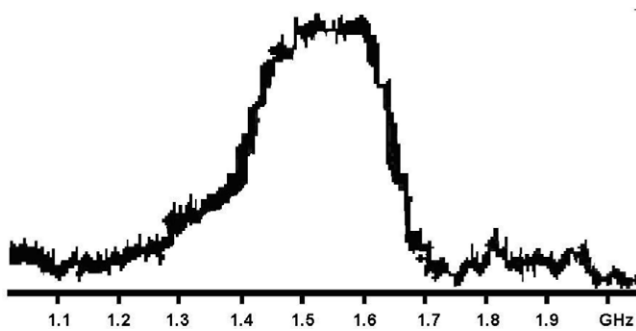

Figure 11. The digitized oscilloscope trace of the amplitude–frequency distribution inherent in the acousto-optical cell with collinear heterodyning exploiting the longitudinal elastic waves of finite amplitude in a lead molybdate crystal.

$\gamma \in [1.04, 1.20]$ had been experimentally realized. During the experiments, we have placed a diaphragm at about 5 mm from the vicinity of the piezoelectric transducer area (about 13.5% of the total aperture) to minimize the effect of this area, where an increase in the power of difference-frequency waves takes place. Consequently, the working optical aperture of a cell was a little bit longer than 37 mm. The bandwidth of that prototype was about 180 MHz. The efficiency of light scattering by an additional acoustic wave at the difference-frequency was slightly exceeding 1%. Figure 11 shows the digitized oscilloscope traces of the amplitude–frequency distribution peculiar to that prototype with the acousto-optical cell based on the collinear wave heterodyning. The digitized trace of this distribution had been recorded by a multi-pixel CCD linear array camera through connecting the input signal port of a cell to an ultra-high-frequency radio-wave sweep generator and fulfilling the acoustic wave heterodyning in a lead molybdate crystal. For a radio-wave signal, producing the dynamic acoustic grating on the resulting carrier difference frequency of about 235 MHz, the attenuation is close to 3 dB over the total cell aperture. At the same time, for the signal acoustic waves at even the lower original frequency 1440 MHz the attenuation exceeds 100 dB along a 37 mm aperture, which is perfectly unacceptable in practice. Within the second set of our
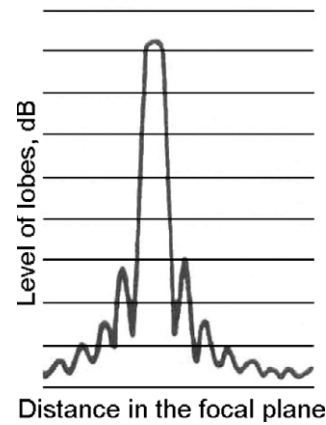
experimental tests, we examined the resolution of the spectrum analyzer with the cell exploiting the collinear acoustic wave heterodyning. In fact, the intensity distribution of an individual resolvable spot in the focal plane of the integrating lens had been considered. In so doing, the technique, which had long been in use, with a very narrow slit diaphragm scanning over a sufficiently sensitive photodetector and subsequent logarithmic amplifier was applied to our needs. In practice, this technique gives us an opportunity to fix the continuous distribution of light intensity in the lobes of an individual spot really carefully in a rather wide dynamic range of about 25 dB [11]. One can see that the measured level of the first lobes lies at a level of about -13 dB with initially homogeneous lighting of the operating cell's aperture, which is in good coincidence with the well-known theoretical prediction [12]. Figure 12 presents the digitized trace, which had been recorded in the focal plane of the integrating lens, see figure 7, via applying just a single-frequency excitation at the input signal port of the proposed cell. In the case under consideration, the physical limit of the frequency resolution is $V/D \approx 98$ kHz, while the experimentally obtained value, affected by acoustic losses as well as by technical imperfections of the integrating lens, corresponds to a frequency resolution of about $\delta f \approx 120$ kHz at a level of -10 dB and gives the number of resolvable spots or, which is the same, the number of parallel frequency channels $N \approx 1500$. By this is meant that the proposed technique for direct parallel optical spectrum analysis of gigahertz-frequency range radio-wave signals provides at least 1500-channel processing even within our proof-of-principle experiment. As this takes place, the accuracy or the relative frequency resolution $\delta f / f_{LS}$ (where $f_{LS} = 1444$ MHz) is less than 10^{-4}, which is practically unattainable for conventional direct acousto-optical methods of spectrum analysis.

6. Brief comparative discussion

In this step, it seems quite reasonable to compare operational characteristics of the proposed acousto-optical cell with the

corresponding characteristics of an acceptable traditional high-frequency cell. Let us take a cell exploiting longitudinal acoustic waves along the X axis of such a low-loss crystal as lithium niobate with $M_2 = 7.0 \times 10^{-18}$ s^3 g^{-1}, $\Gamma = 0.15$ dB cm^{-1} GHz^{-2} and $V_L = 6.57 \times 10^5$ cm s^{-1}. Each cell can be characterized in both frequency and amplitude domains. The best set of frequency characteristics for the chosen cell at the central frequency $f_0 = 1.5$ GHz includes the frequency bandwidth $\Delta f \approx f_0/2 = 750$ MHz, the upper signal frequency $f_U = 1875$ MHz, the optical aperture $D_0 = 3$ (dB)/(Γf_U^2) ≈ 5.7 cm associated with a 3 dB level of acoustic losses at the frequency f_U, the frequency resolution $\delta f = V/D_0 = 115$ kHz, the number of resolvable spots $N = \Delta f/\delta f \approx 6520$ and the relative accuracy of analysis $\delta f/f_0 \approx 0.77 \times 10^{-4}$. The efficiency of this cell with $L = 1.0$ cm and a given exciting acoustic wave power density P_0 can be estimated by $I_0 = \sin^2(q_0 L)$, where q_0 can be taken from equation (5*b*) at $\lambda = 532$ nm. To make the comparison with the data at the end of section 2, let us take $I_0 = 0.03$, i.e. 3%. In this case, one can estimate $q_0 = I^{1/2}/L \approx 0.173$ cm^{-1} and $P_0 = (2I\lambda^2)/(\pi^2 L^2 M_2) \approx 0.25 \times 10^7$ g s^{-3} = 0.25 W cm^{-2}. Thus, the traditional LiNbO$_3$ cell looks, at first glance, slightly preferable than the above-proposed one. Nevertheless, to make the correct conclusion one has to take into account a few following circumstances. First, a large optical aperture requires growing a large enough boule of lithium niobate. It should be a mono-domained svilen-less single crystal exhibiting a high optical homogeneity and providing top-level conditions for propagation of both optical as well as UHF acoustic waves through a large-aperture cell. In practice, it is rather difficult to satisfy these requirements, but in another case, a similar cell will have lost a significant part of its potential frequency resolution. Second, designing a truly effective piezoelectric transducer with a 50% frequency bandwidth at a carrier frequency of about 1.5 GHz is not an ordinary task. The existing difficulties in the technology of production as well as in subsequent acoustic and electronic matching of a similar wide-band piezoelectric transducer can be resolved currently only by decreasing its efficiency and/or narrowing its bandwidth. This is why the above-noted potential frequency characteristics have to be considered as just the limiting theoretical values. Third, the estimated efficiency for a lithium niobate cell cannot be applied directly to the comparison under consideration, because the proposed new cell involves two cascades of processing and provides an additional function, namely the heterodyning, which needs naturally additional power consumption. Then, during this comparison one has to take into account that our experimentally tested lead molybdate cell had not been really optimized, because the main purposes of this cell were to demonstrate a new principle of operation as well as to exhibit that it can be realized practically with more or less acceptable operational characteristics. Furthermore, in parallel with performing the cell's optimization more effective acoustically and acousto-optically materials, such as KRS-5 [13], can be examined within the proposed technique in expecting much better performance data. Together with this the proposed technique of spectral analysis, which includes the developed cell with two piezoelectric transducers and the

frequency-dependent preamplification, should be in principle compared with the simplest technique based on preliminary electronic mixing of the high-frequency radio-wave signals with further launching of the resulting acoustic wave at the difference frequency. However, this kind of comparison evidently exceeds the limits of this paper as, on the one hand, it is mostly related to comparing electronic rather than acousto-optical components of the functional scheme under consideration and, on the other hand, one needs more practical experience of exploiting the proposed technique than he has at the moment to make such a comparison really qualitatively.

7. Conclusion

The presented data demonstrate both the possibility and the potential advantages of applying a co-directional collinear wave heterodyning to an essential, about an order of magnitude, improvement of the frequency resolution within a multi-channel parallel acousto-optical spectrum analysis of gigahertz-frequency-range analog radio-wave signals. In so doing, we have theoretically investigated the phenomenon of a co-directional collinear wave heterodyning, taken in the particular case of mixing the longitudinal acoustic waves of finite amplitudes. Then, an opportunity of implementing acousto-optical data processing with the wave heterodyning has been experimentally performed utilizing the specially designed acousto-optical cell made of a lead molybdate single crystal. Together with this, the methods for estimating the total efficiency of operation and optimizing aperture parameters for a new type of cell have been developed. Moreover, the phenomenon of affecting the light distribution inherent in an individual resolvable spot by joint action of the incident light bean non-uniformity and the natural presence of acoustical losses along the cell's optical aperture has been estimated. The proposed technique exploits a two-cascade algorithm of processing and is intended for direct parallel and precise optical spectrum analysis and provides about 1500 frequency channels for processing analog radio-wave signals in a gigahertz-frequency range with an accuracy or, what is the same, with a relative frequency resolution better than 10^{-4}, which is usually unattainable for conventional direct acousto-optical methods. The obtained results reflect the fruitful character of modern approaches based on applying various nonlinear phenomena to improving the performance data of optical processing and giving an appropriate example of this kind. At the moment, a few practical advantages of the presented approach can be noted. First, the proposed device does not need additional electronic equipment for mixing the signals and selecting the resulting carrier frequency, because heterodyning can be performed directly in a cell and provides potentially a dynamic range of about 90 dB, peculiar to wave processes in solids. Then, the approach under consideration decreases the required relative bandwidth of the piezoelectric transducer from 50–100% at the resulting frequency within a conventional cell to 10–15% at the initial carrier frequency. Within our proof-of-principle experiment the acousto-optical cell with two piezoelectric transducers

was used, but generally it is not necessary. Due to the relative bandwidth not exceeding 15%, potentially it is quite reasonable to exploit just one transducer. Thirdly, in the case of a spatially multi-channel arrangement of the acousto-optical cell, the identity of neighboring spatial channels to each other can be provided by adjusting the corresponding heterodynes. Finally, one should note that the number of isotropic or crystalline materials, which are appropriate for acousto-optical cell processing signals in a gigahertz-frequency range, are definitely restricted due to the fast-growing influence of a square-law frequency dependence for the acoustic attenuation in solids. For instance, one can easily show [6, 7] that the above-discussed lead molybdate crystal cannot be used for creating a conventional acousto-optical cell operating with signals whose carrier frequency exceeds about 300–400 MHz. Nevertheless, just this crystalline material had been exploited for control over 1.5 GHz signals within these studies. Consequently, one can conclude that a two-cascade arrangement of a cell presented here allows extending the spectrum of the acousto-optical materials being appropriate for direct processing of ultra-high-frequency analog radio-wave signals.

Acknowledgments

References

[1] Kivshar Yu S and Agrawal G P 2003 *Optical Solitons: from Fibers to Photonic Crystals* (New York: Academic)
[2] Akhmediev N N and Ankiewich A 1997 *Solitons: Nonlinear Pulses and Beams* (London: Chapman and Hall)
[3] Shcherbakov A S and Aguirre Lopez A 2006 Wave multiplication of binary encoded data exploiting solitary multi-pulse non-collinear three-wave coupled states *J. Opt. A: Pure Appl. Opt.* **8** 464–72
[4] Dirac P A M 1999 *The Principles of Quantum Mechanics* 4th edn (Oxford: Oxford University Press)
[5] Dodd K, Eilbeck J C, Gibbon J D and Morris H 1984 *Solitons and Nonlinear Wave Equations* (Orlando: Academic)
[6] Blistanov A A 2007 *Crystals for Quantum and Nonlinear Optics* (Moscow: MISIS)
[7] Dmitriev V G, Gurzadyan G G and Nikogosyan D N 1999 *Handbook of Nonlinear Optical Crystals* 3rd edn (Berlin: Springer)
[8] Das P D and DeCusatis C M 1991 *Acousto-Optic Signal Processing: Fundamentals & Applications* (Boston: Artech House)
[9] Klein R W and Cook B D 1967 A unified approach to ultrasonic light diffraction *IEEE Trans.* **SU-14** 123–34
[10] Born M and Wolf E 1970 *Principles of Optics* 3rd edn (Oxford: Pergamon)
[11] Shcherbakov A S, Tepichin Rodriguez E, Aguirre Lopes A and Maximov Je 2009 Frequency bandwidth and potential resolution of optical modulators exploiting a multi-phonon light scattering in crystals *Opt.: Int. J. Light Electron Opt.* **120** 301–12
[12] Goodman J W 1996 *Introduction to Fourier Optics* 2nd edn (New York: McGraw-Hill)
[13] Shcherbakov A S, Maximov Je and Sanchez Lucero D 2010 Potentials of the acousto-optical spectral data processing on the basis of a novel algorithm of the collinear wave heterodyning in a large-aperture KRS-5 crystalline cell *Proc. SPIE* **7598** 75981J